Dynamic Data Driven Multistatic Radio Frequency Imaging

Jia Li, *Senior Member, IEEE,* Robert Ewing, *Fellow, IEEE,* and Erik Blasch, *Fellow, IEEE*

***Abstract*—Multistatic radio frequency (RF) imaging systems utilize distributed RF sensors which transmit waveforms to illuminate a target scene and estimate the dielectric properties of the region of interest from the received echoes. This study applies the principles of dynamic data driven systems to improve the performance of multistatic RF imaging system in terms of power efficiency and image reconstruction accuracy. Target location information derived from initial image reconstruction is applied to dynamically reconfigure the imaging system. Based on the geolocation of targets relative to the distributed RF sensors, Fisher information matrices associated with the targets and multistatic sensor pairs are calculated and applied to derive optimum power allocation strategies under different constraints. Image reconstruction of multistatic RF imaging often suffers from artifacts and ghost targets caused by multipath propagation and multi-order reflections. A grouped-coordinate descent (GCD) type reconstruction algorithm is developed to exploit target location information. The iterative optimization alternates between the groups of target space parameters and non-target space parameters. The dictionary of reconstruction is dynamically updated to include the secondary reflections from target locations. The improved model fidelity leads to more accurate reconstructions without a significant increase in computational complexity. Numerical simulations demonstrate that the proposed power allocation strategies are effective in energy saving. The proposed reconstruction algorithm converges faster than sequential parameter update algorithms, and the reconstruction accuracy is superior to that using a fixed dictionary containing the first order reflections only.**

***Index Terms*—radio frequency imaging, power allocation, image reconstruction, multipath propagation, multistatic radar, sensor fusion, dynamic data driven application**

I. Introduction

RADIO frequency (RF) imaging is a challenging problem that has attracted intensive research interests due to its potential applications in defense, homeland security and automotive industry [1]–[4]. Through the wall imaging, surveillance of large areas and autonomous driving are some applications of RF imaging, which is an inverse scattering problem and has similarities to computed tomography in the medical domain [5]. The imaging mechanism is to illuminate the target scene using RF pulses and infer the dielectric properties of the region from the scattered waveforms recorded. For multistatic imaging systems, RF sensors are distributed in multiple locations and the reconstruction algorithm must integrate the information from all sensor pairs. From system design and configuration to reconstruction algorithms, there are many challenges to address to improve the performance of RF imaging systems. This paper investigates power allocation policies and reduction of reconstruction artifacts using principles of dynamic data driven applications systems (DDDAS).

DDDAS methods have long been applied to solve problems in the fields of science and engineering, and have seen rapid advancements in sensing, machine learning, and information security in recent years [6], [7]. DDDAS can be adaptive to both system input and output in real-time to improve system performance. The basic process of DDDAS is to monitor the key measurements or system output related to system performance; design an objective function that reflects the relationship between the system performance, the system parameters and the measurements, such as a feedback loop; and to adjust the system parameters based on the optimization of the objective function. The implementation is usually in real-time. A system dynamically driven by real-time data has many advantages over systems with fixed configuration. The benefits include: optimal resource allocation, such as bandwidth usage and power consumption; increased accuracy of system output, such as signal reconstruction quality; dynamic user access, such as spectrum monitoring based access control; and adaptive decision making. Reconstruction in an RF imaging system was traditionally offline due to the high computational complexity. However, advanced hardware implementation, such as high-end field programmable gate array (FPGA) dedicated to each sensor, and fiber-optics cables connecting sensors and control center that provide large bandwidth for real-time communications, allows real-time system adaptation and image reconstruction. This motivates us to develop more adaptive imaging system based on the DDDAS concept for radar systems [8].

The first issue addressed in this paper is power allocation in multistatic RF imaging. When RF sensors are distributed in multiple locations, the imaging system can exploit channel diversities to improve the quality of reconstruction. The diversity may include, but not limited to, waveform, channel noise, scatterer and attenuation along propagation paths [9], [10]. An optimum sensor management policy should be developed to effectively exploit the diversity in multistatic imaging system [11]. Sensor management has been an active research area in the last couple of decades [12]–[16], where power efficiency is a main issue investigated in resource-aware management. When sensors are off-grid and have to operate over long period, it's critical to have an efficient power allocation strategy to increase the system's sustainability. Even if sensors are on the power grid, power consumption should still be

J. Li is with the Department of Electrical and Computer Engineering, Oakland University, Rochester, MI, 48309 USA e-mail: li4@oakland.edu.

R. Ewing is with Sensors Directorate, Air Force Research Laboratory, WPAFB, OH, 45433 USA e-mail: robert.ewing.2@us.af.mil

E. Blasch is with Information Directorate, Air Force Research Laboratory, Rome, NY, 13441 USA email: erik.blasch.1@us.af.mil

managed to reduce spectrum contamination and probability of interception by an adversary. In [17], optimal power allocation in multistatic radar and communication system was investigated towards low probability of intercept. The objective is to minimize total power consumption while maintaining certain target detection probability and information rate. Yan et al. studied radar sensor selection and power allocation for multiple target tracking under the constraint of tracking accuracy in [18]. Cramér-Rao lower bound (CRLB) was used as a performance metric to quantify the tracking performance in the study. Optimization of sensor configuration other than power allocation has also been widely studied. For example, the optimization of sparse aperture configuration was recently investigated for millimeter-wave imaging in [19].

We propose *power allocation strategies* using Fisher information associated with target reflectivities based on target location information derived from initial sensing. As seen in [18] and will be discussed in Section III-A, Fisher information is a commonly used performance metric. Two scenarios were considered in our study. One minimizes the mean squared error of target reflectivity estimators given a fixed power budget, while the other minimizes the total power consumption given required reconstruction accuracy. Our analysis shows that the first scenario corresponds to a nonconvex optimization problem, for which gradient based optimization algorithm was developed to get solutions. The second scenario leads to a convex optimization problem with linear objective and nonlinear constraint, which can be solved efficiently with existing convex optimization toolbox. Numerical experiments show that the optimal power allocation strategies driven by target location information are more efficient than uniform allocation and greedy allocation in both scenarios.

When a RF waveform propagates from transmitter to receiver, it may be scattered multiple times and reach the receiver through different paths. The propagation paths are usually determined by the locations of scatterers in the scene. This is the well-known multipath propagation phenomenon in RF imaging. As an inverse problem, RF imaging is solved through optimization procedure. Its objective function is determined by the system model and the metric used. Multipath propagation can be modeled by including multiple levels of scattering in the system model. For example, Leigsnering has investigated multipath propagation in through-the-wall radar imaging [20], [21]. The reflections from surrounding walls are modeled using prior knowledge of the location and thickness of walls. In [22], ghost images caused by multipath propagation have been exploited in radar target classification. In both studies, the locations of higher order scatterers are assumed to be known so the system models were predetermined and fixed throughout the reconstruction process.

This paper considers reconstructing reflectivity of point targets in free space. Each target is not only a first order scatterer, but also a higher order scatterer on the propagation paths of waveforms reflected from other targets. When the number of targets and their locations are unknown, a naive approach to model multipath propagation is to include every pixel of the image as both first order scatterer and higher order scatterer in the system model. However, such an exhaustive approach can cause the size of reconstruction dictionary to grow exponentially with the image size and lead to significant increase in reconstruction complexity. To maintain the computational cost at a practical level, we propose to exploit the target location information and update the reconstruction dictionary dynamically to include secondary reflections from targets only. This is a data-driven model reduction strategy which generates adaptive model from data obtained during online computation. Such strategies have been studied before to reduce computational cost in inverse problems [23], to adapt reduced models from incomplete data [24], and to assist real-time decision making [25]. The target location information is also used to develop a *grouped-coordinate descent* type algorithm for the reconstruction. In each iteration, the optimization alternates between the parameter domains of target space and non-target space. The results show that the proposed algorithm converges faster than sequential single coordinate descent algorithm, and the dynamic dictionary improves system model fidelity and reduces artifacts caused by multipath propagation with low computational cost.

There are three contributions of this paper.

1) Fisher information collected by multistatic RF sensors with respect to target reflectivity parameters is derived. Optimal power allocation strategies based on Fisher information are proposed for different scenarios and the corresponding optimization algorithms are developed.
2) A grouped-coordinate descent type algorithm is developed for the reconstruction of multistatic RF imaging system. The target location information allows dynamic update of reconstruction dictionary to include secondary reflections from targets, and iterative optimization that alternates between target space and non-target space parameters. The algorithm is not only effective to reduce artifacts caused by multipath propagation, but also has a faster convergence rate and lower computational complexity.
3) The target-aware RF imaging system demonstrates how dynamic data driven methods can be applied to sensor management and model reduction.

The rest of the paper is organized as follows. In Section II, the system model of RF imaging is introduced. Section III derives Fisher information based dynamic power allocation strategies. The reconstruction algorithm with dynamic dictionary is described in Section IV. Numerical simulations of the proposed data-driven strategies and the results are presented in Section V. Section VI concludes the paper and discusses future work.

II. System Model

Multistatic RF imaging system is composed of distributed RF sensors to achieve spatial diversity. The sensors can be either homogeneous transceivers or heterogeneous transmitters and receivers. To create an image, RF pulses are transmitted to illuminate regions of interest and the echoes recorded at different locations are processed to estimate dielectric properties of the regions and detect targets located within the regions. The imaging system can use a discrete set of frequency components

suitable for the environment of the region. For example, in underground target imaging, the electromagnetic wave must be able to penetrate the ground and the choice of frequency depends on the type of soil and target depth [2]. This paper considers free space waveform propagation for ground targets and airborne targets detection, where waveform frequency can be chosen according to desired image resolution. For simplicity of the model, it's also assumed that reflection at each location is isotropic so that the reflectivity may vary with frequency, but not angle.

Consider a multistatic imaging system composed by M transmitters and N receivers distributed in an area $\mathcal{A} \in \mathbb{R}^2$. The reflectivity of the region of interest is a function $\theta : \mathcal{A} \to \mathbb{R}$. The shadowing on a bistatic link caused by environment can be modeled as a weighted integral of $\theta(\mathbf{x})$ over $\mathcal{A}$ [26], [27]. The goal of the imaging system is to estimate θ by processing the recorded echoes. To discretize the parameter space, let $\mathbf{x}_i$ be the coordinates of the i-th pixel of the image to be reconstructed, and $\theta_i := \theta(\mathbf{x}_i)$ be the reflectivity of $\mathbf{x}_i$. The estimation of θ is converted to estimate $\boldsymbol{\theta} = [\theta_1, \theta_2, \ldots, \theta_K]^T$, a K-dimensional parameter vector, where K is the total number of pixels in the image.

A. First order model

A transmitted waveform can be reflected by multiple scatterers and multiple times before reaching receivers, known commonly as multipath propagation. For the (m, n)-th bistatic link, the first order model assumes waveform transmitted by the m-th transmitter is reflected by the scatterers in the field only once before reaching the n-th receiver. Assuming orthogonal channels, the baseband measurement obtained by the (m, n)-th bistatic link, $y_{mn}(t)$, is a combination of the first order echoes [1],

$$y_{mn}(t) = \sum_{i=1}^{K} \sqrt{a_{mn}(\mathbf{x}_i)p_m}\theta_i s_m(t - \tau_{mn}(\mathbf{x}_i))\cdot e^{-j\phi_{mn}(\mathbf{x}_i)} + \omega_{mn}(t) \quad (1)$$

where $s_m(t)$ is the baseband pulse of unit energy used by the m-th transmitter, $a_{mn}(\mathbf{x}_i)$ is the path loss associated with $\mathbf{x}_i$, p_m is the transmission power of the m-th transmitter, $\tau_{mn}(\mathbf{x}_i)$ is the bistatic propagation delay associated with $\mathbf{x}_i$, $e^{-j\phi_{mn}(\mathbf{x}_i)}$ is the phase offset between the transmitter and receiver caused by the reflection at $\mathbf{x}_i$, and $\omega_{mn}(t)$ is the zero mean, additive white Gaussian noise of the channel. Let $\tilde{\mathbf{x}}_m$ be the coordinates of the m-th transmitter and $\check{\mathbf{x}}_n$ be the coordinates of the n-th receiver. The path loss $a_{mn}(\mathbf{x}_i)$ is proportional to $\frac{1}{d^2(\tilde{\mathbf{x}}_m, \mathbf{x}_i)d^2(\mathbf{x}_i, \check{\mathbf{x}}_n)}$, where $d(\mathbf{x}, \mathbf{x}') = \|\mathbf{x} - \mathbf{x}'\|$ is the Eucleadian distance between $\mathbf{x}$ and $\mathbf{x}'$. The propagation delay $\tau_{mn}(\mathbf{x}_i)$ is determined by

$$\tau_{mn}(\mathbf{x}_i) = \frac{d(\tilde{\mathbf{x}}_m, \mathbf{x}_i) + d(\mathbf{x}_i, \check{\mathbf{x}}_n)}{c}, \quad (2)$$

where c is the speed of light. The phase $\phi_{mn}(\mathbf{x}_i)$ is determined by the length of propagation path as well as the scatterer located at $\mathbf{x}_i$. Please note the waveform propagated through direct path is not included in Eq. (1) because it is usually removed in the preprocessing step.

B. Second order model

The first order model in Eq. (1) doesn't include higher order reflections. However, when targets in the scene have strong reflectivity, the strength of second order reflections may be comparable to first order reflections. If system model doesn't distinguish second order reflections from first order reflections, the reconstructed images may have serious artifacts or even "ghost targets". To improve the accuracy of image reconstruction, higher order reflections should be included in the system model. Eq. (1) is modified to introduce the second order reflections,

$$y_{mn}(t) = \sum_{i=1}^{K} \sqrt{a_{mn}(\mathbf{x}_i)p_m}\theta_i s_m(t - \tau_{mn}(\mathbf{x}_i))e^{-j\phi_{mn}(\mathbf{x}_i)} + \sum_{i=1}^{K}\sum_{j=1, j\neq i}^{K} \sqrt{a_{mn}(\mathbf{x}_i, \mathbf{x}_j)p_m}\theta_i\theta_j s_m(t - \tau_{mn}(\mathbf{x}_i, \mathbf{x}_j))\cdot e^{-j\phi_{mn}(\mathbf{x}_i, \mathbf{x}_j)} + \omega_{mn}(t) \quad (3)$$

where $a_{mn}(\mathbf{x}_i, \mathbf{x}_j)$ corresponds to the path loss along $\tilde{\mathbf{x}}_m \to \mathbf{x}_i \to \mathbf{x}_j \to \check{\mathbf{x}}_n$, $\tau_{mn}(\mathbf{x}_i, \mathbf{x}_j)$ is the propagation delay and $\phi_{mn}(\mathbf{x}_i, \mathbf{x}_j)$ is the phase offset associated with the path. To strike a balance between accuracy and complexity of the system model, reflections of orders higher than the second order are deemed insignificant and not included in the model.

C. Discrete system model

The system model shown in Eq. (3) can be discretized by sampling the transmitted waveforms, the received echoes and the noise process:

$$\mathbf{y}_{mn} = \sqrt{p_m}\mathbf{D}_{mn}\boldsymbol{\theta} + \sqrt{p_m}\tilde{\mathbf{D}}_{mn}\mathbf{v}(\boldsymbol{\theta}) + \boldsymbol{\omega}_{mn} \quad (4)$$

where $\mathbf{y}_{mn}$ is the vector representing the sampled echoes, $\mathbf{D}_{mn}$ and $\tilde{\mathbf{D}}_{mn}$ are matrices whose columns are the attenuated pulses received along the paths of the first order reflections and the second order reflections, separately, and $\boldsymbol{\omega}_{mn}$ is the sampled noise vector. $\mathbf{v}(\boldsymbol{\theta})$ is a $\frac{K(K-1)}{2} \times 1$ vector formed from the distinct nondiagonal elements of the $K \times K$ matrix $\boldsymbol{\theta}\boldsymbol{\theta}^T$, i.e. $\mathbf{v}(\boldsymbol{\theta}) = [\theta_1\theta_2, \theta_1\theta_3, \ldots, \theta_{K-1}\theta_K]^T$. $\mathbf{D}_{mn}$ and $\tilde{\mathbf{D}}_{mn}$ are called the first order dictionary and the second order dictionary of the (m, n)-th bistatic link. The dictionaries can be pre-calculated and stored for each bistatic link of the imaging system.

III. Dynamic Power Allocation

For multistatic radio frequency imaging, the objective is to obtain the most accurate estimation of reflectivity of the targets in the scene. As the signal to noise ratio (SNR) of a waveform propagation channel is directly affected by the power of the transmitted pulses, power allocation policy has a direct impact to the quality of reconstructed images. Thus, the investigation of dynamic power allocation policy under different constraints is one of the major subjects of this paper.

Dynamic power allocation in a multistatic radio frequency imaging system is a task of sensor management. Optimal configuration is critical to sensor systems operating under resource

This article has been accepted for publication in a future issue of this journal, but has not been fully edited. Content may change prior to final publication. Citation information: DOI 10.1109/TAES.2021.3098160, IEEE Transactions on Aerospace and Electronic Systems

constraints. System optimality varies with sensor, environment and target (SET) operational conditions. For example, power efficiency is the key to long-term sustainability for off-grid RF imaging system. Minimizing power consumption is also necessary to reduce spectrum contamination in an urban environment, and to achieve low probability of intercept.

A. Fisher information gain

Choosing an optimal configuration of a sensor system from a high dimensional system parameter space is not a trivial problem. Information based sensor management have been well studied and widely applied to assess the system's fundamental limitations [28]–[30]. The general principle is that sensors should be scheduled and resources should be allocated to extract the maximum amount of relevant information. To quantify and optimize the information collection capability of sensors, various information measures, such as entropy [31], Fisher information [32], [33], mutual information [34], and Kullback-Leibler divergence [35], have been applied in the design of risk or reward functions [36].

By assuming additive white Gaussian noise for all the propagation channels, the probability density functions of $\mathbf{y}_{mn}$ conditioned on the value of $\boldsymbol{\theta}$, is

$$f(\mathbf{y}_{mn};\boldsymbol{\theta}) = \frac{1}{(2\pi\sigma_\omega^2)^{L/2}} e^{-\frac{|\mathbf{y}_{mn}-\sqrt{p_m}\mathbf{D}_{mn}\boldsymbol{\theta}|^2}{2\sigma_\omega^2}} \tag{5}$$

where σ_ω^2 is the variance of Gaussian noise, which is assumed to be the same for all channels, and L is the dimension of $\mathbf{y}_{mn}$. Please note the conditional probability given in Eq. (5) is based on the first order system model to simplify the derivation of power allocation strategies and reduce the computational complexity of the optimization procedure. With the parametric model in Eq. (5), image reconstruction can be formulated as a maximum likelihood estimation of $\boldsymbol{\theta}$. For a maximum likelihood estimator, its mean squared error is going to approach Cramér-Rao lower bound (CRLB) asymptotically. As the CRLB can be obtained through the inverse of Fisher information matrix, the power allocation strategies developed in this paper are based on the Fisher information gain.

As shown in Appendix A, the Fisher information matrix of the (m,n)-th bistatic link with respect to $\boldsymbol{\theta}$ is

$$\mathcal{I}_{mn}(p_m,\boldsymbol{\theta}) = \frac{p_m \mathbf{D}_{mn}^T \mathbf{D}_{mn}}{\sigma_\omega^2} \tag{6}$$

which implies the information gain over θ_i is proportional to the transmission power p_m, and the attenuation coefficient $a_{mn}(\mathbf{x}_i)$ which is the i-th diagonal element of the $K \times K$ matrix $\mathbf{D}_{mn}^T \mathbf{D}_{mn}$. Fig. 1 shows the attenuation maps formed by two bistatic sensor pairs over the same region. Pixel intensity of the images equals $a_{mn}(\mathbf{x}_i)$. Note that the attenuation map is equivalent to Fisher information gain map if transmission and noise powers are the same for both links. It's obvious that each sensor pair forms a unique attenuation map, which is determined by the sensor locations relative to the physical locations of the image pixels. For any bistatic sensor pair, the closer $\mathbf{x}_i$ is to a transmitter or a receiver, the more information can be collected with respect to θ_i by the sensor pair. Closely distributed bistatic sensor pairs can collect more information with respect to their neighborhoods than greatly distanced sensor pairs.

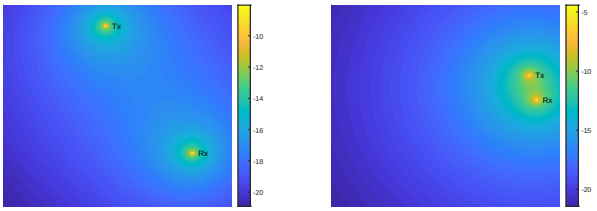

(a) (b)

Fig. 1: Attenuation maps of two bistatic sensor pairs.

As users of RF imaging system usually focus on specific targets, it is reasonable to reconfigure the system to achieve more accurate estimation of targets' reflectivity. The intuitive idea is that power should be allocated to transmitters that are close to targets to increase Fisher information gain over target reflectivity. At the initial stage of sensing, target locations are unknown. Power is distributed equally among all transmission sensors. The initial sensing and reconstruction can give an estimate of target locations. Targets of interests are most likely to have high value of reflectivity. So a threshold θ_{min} can be applied over the reconstructed image, and the set of pixels whose reflectivity is greater than θ_{min} are regarded as targets or clutters. Let S be the index set corresponding to such a target set, i.e. $S := \{i|\theta_i > \theta_{\text{min}}, i = 1 \dots K\}$. Let the cardinality of S be q. We use $\boldsymbol{\theta}_S$ to denote the q dimensional vector consisting of the elements of $\boldsymbol{\theta}$ indexed by the member of S. The set $\bar{S} = \{1,2,\dots,K\} - S$ denotes the complement of S intersected with $\{1,\dots,K\}$. In Section III-B, power allocation strategies are derived under two different constraints based on the Fisher information matrix of $\boldsymbol{\theta}_S$.

B. Dynamic power allocation

Optimal power allocation policies under two scenarios are investigated in this paper. In the first scenario, the imaging system has a fixed total power budget and power shall be allocated among sensors to minimize mean squared error of $\hat{\boldsymbol{\theta}}_S$. In the second scenario, the aim is to use minimal power to achieve a required accuracy of $\hat{\boldsymbol{\theta}}_S$.

1) Mean Squared Error Minimization: Let P represent the total power available to the imaging system, and $\mathbf{p} = (p_1, p_2, \dots, p_M)^T$ be the power allocation among M transmitters. After the initial sensing, the index set of targets S is estimated by thresholding the reconstructed image $\boldsymbol{\theta}$. The goal is to minimize the mean squared error (MSE) of $\hat{\boldsymbol{\theta}}_S$, which is bounded by the inverse of Fisher information matrix $\mathcal{I}^{-1}(\mathbf{p},\boldsymbol{\theta}_S)$ for maximum likelihood estimation. So the proposed optimum allocation scheme minimizes the trace of

This article has been accepted for publication in a future issue of this journal, but has not been fully edited. Content may change prior to final publication. Citation information: DOI 10.1109/TAES.2021.3098160, IEEE Transactions on Aerospace and Electronic Systems

$\mathcal{I}^{-1}(\mathbf{p}, \boldsymbol{\theta}_S)$, which can be formulated as

$$\begin{aligned} \min_{\mathbf{p}} \quad & \text{tr}(\mathcal{I}^{-1}(\mathbf{p}, \boldsymbol{\theta}_S)) \\ s.t. \quad & \sum_{m=1}^{M} p_m = P \\ & p_m \geq 0 \qquad m = 1 \dots M \\ & p_m \leq p_{max} \qquad m = 1 \dots M \end{aligned} \tag{7}$$

where p_{max} is the maximum power available to each sensor. As the objective function is nonconvex, this is a nonconvex optimization problem of which a global minimum is not easy to obtain with low complexity algorithms [37]. Grid search suffers from the curse of dimensionality as the number of trials grows exponentially with the number of transmitters in the imaging system. While random search is theoretically more efficient than grid search in high dimensional space, it may still require hundreds of trials to achieve desired accuracy [38]. We aim to develop a local minimum search algorithm that is likely to approach global minimum via a good initialization.

A heuristic idea is to allocate power among sensors to collect equal amount of Fisher information with respect to each element in $\boldsymbol{\theta}_S$. By Eq. (14) in Appendix, Fisher information of θ_i is

$$\mathcal{I}(\mathbf{p}, \theta_i) = \frac{1}{\sigma_\omega^2} \sum_{m=1}^{M} p_m [\mathbf{B}_m]_{i,i} \tag{8}$$

where $\mathbf{B}_m := \sum_{n=1}^{N} \mathbf{D}_{mn}^T \mathbf{D}_{mn}$, and $[\mathbf{B}_m]_{i,i}$ is the diagonal element of $\mathbf{B}_m$ corresponding to θ_i. The heuristic approach will lead to a linear system of equations, $\{\sum_m p_m [\mathbf{B}_m]_{i,i} = 1, i \in S\}$. As the cardinality of S is q, the system has a total of q equations. If $q \geq M$, the system is either fully determined or overdetermined, and has an analytic solution to its least squares formulation. If $q < M$, the system is underdetermined. A greedy method can be applied to reduce the number of unknowns, which finds the transmitter closest to each target and only keeps these transmitters in the system. The greedy method reduces the number of unknowns to be less than or equal to q and the system will again have an analytic solution. Finally, the solution to the linear system of equations is scaled to satisfy the constraint of $\sum_{m=1}^{M} p_m = P$.

The heuristic solution is applied to initialize a gradient-based algorithm to find the local minimum of the objective function in Eq. (7), which is detailed in Algorithm 1.

Algorithm 1 Power allocation to minimize MSE of $\boldsymbol{\theta}_S$

1: **Input:** $\{\mathbf{B}_m\}$, S, N_{iter}, ϵ,
2: **Init:** $\mathbf{p}^{(0)}$, step $\alpha^{(0)}$
3: **while** $i < N_{iter}$ and $|\mathbf{p}^{(i)} - \mathbf{p}^{(i-1)}| > \epsilon$ **do**
4: $\quad \mathbf{p}^{(i)} = \mathbf{p}^{(i-1)} - \alpha^{(i-1)} \nabla \text{tr}\left(\mathcal{I}^{-1}(\mathbf{p}^{(i-1)}, \boldsymbol{\theta}_S)\right)$ s.t. $p_m \geq 0$ and $p_m \leq p_{max}$
5: $\quad \mathbf{p}^{(i)} = \frac{\mathbf{p}^{(i)} * P}{\sum_m p_m^{(i)}}$
6: $\quad \alpha^{(i)} = \frac{\left|(\mathbf{p}^{(i)} - \mathbf{p}^{(i-1)})^T \cdot \left[\nabla \text{tr}\left(\mathcal{I}^{-1}(\mathbf{p}^{(i)}, \boldsymbol{\theta}_S)\right) - \nabla \text{tr}\left(\mathcal{I}^{-1}(\mathbf{p}^{(i-1)}, \boldsymbol{\theta}_S)\right)\right]\right|}{\left|\nabla \text{tr}\left(\mathcal{I}^{-1}(\mathbf{p}^{(i)}, \boldsymbol{\theta}_S)\right) - \nabla \text{tr}\left(\mathcal{I}^{-1}(\mathbf{p}^{(i-1)}, \boldsymbol{\theta}_S)\right)\right|^2}$
7: $\quad i = i + 1$
8: **end while**
9: **Output:** $\mathbf{p}^{(i)}$

The gradient of $\text{tr}(\mathcal{I}^{-1}(\mathbf{p}, \boldsymbol{\theta}_S))$ with respect to p_m is derived as follows.

$$\begin{aligned} & \frac{\partial \text{tr}\left(\mathcal{I}^{-1}(\mathbf{p}, \boldsymbol{\theta}_S)\right)}{\partial p_m} \\ =& \text{tr}\left(\frac{\partial \mathcal{I}^{-1}(\mathbf{p}, \boldsymbol{\theta}_S)}{\partial p_m}\right) \\ =& \text{tr}\left(-\mathcal{I}^{-1}(\mathbf{p}, \boldsymbol{\theta}_S) \frac{\partial \mathcal{I}(\mathbf{p}, \boldsymbol{\theta}_S)}{\partial p_m} \mathcal{I}^{-1}(\mathbf{p}, \boldsymbol{\theta}_S)\right) \\ =& -\frac{1}{\sigma_\omega^2} \text{tr}\left(\mathcal{I}^{-1}(\mathbf{p}, \boldsymbol{\theta}_S) \frac{\partial \left(\sum_{m=1}^{M} p_m \mathbf{B}_{m,\boldsymbol{\theta}_S}\right)}{\partial p_m} \mathcal{I}^{-1}(\mathbf{p}, \boldsymbol{\theta}_S)\right) \\ =& -\frac{1}{\sigma_\omega^2} \text{tr}\left(\mathcal{I}^{-1}(\mathbf{p}, \boldsymbol{\theta}_S) \mathbf{B}_{m,\boldsymbol{\theta}_S} \mathcal{I}^{-1}(\mathbf{p}, \boldsymbol{\theta}_S)\right) \end{aligned} \tag{9}$$

Here $\mathbf{B}_{m,\boldsymbol{\theta}_S}$ is a submatrix of $\mathbf{B}_m$, whose elements are $\{[\mathbf{B}_m]_{i,j}, i, j \in S\}$.

2) Total power minimization: The second scenario considered is to minimize the total power consumption to achieve a required accuracy of $\hat{\boldsymbol{\theta}}_S$, which is specified by the trace of the Fisher information matrix inverse $\text{tr}(\mathcal{I}^{-1}(\mathbf{p}, \boldsymbol{\theta}_S))$. The optimization problem is formulated as

$$\begin{aligned} \min_{\mathbf{p}} \quad & \sum_{m=1}^{M} p_m \\ s.t. \quad & \text{tr}(\mathcal{I}^{-1}(\mathbf{p}, \boldsymbol{\theta}_S)) \leq \eta \\ & p_m \geq 0 \qquad m = 1 \dots M \\ & p_m \leq p_{max} \qquad m = 1 \dots M \end{aligned} \tag{10}$$

where η is the upper bound of the trace of the inverse Fisher information matrix specified by the user. This is a convex optimization problem with linear objective and nonlinear constraint. It can be solved by CVXOPT, a free software for convex optimization [39].

The efficiency of the two power allocation strategies will be demonstrated in Section V. Intuitively, both strategies would allocate more power to the transmitters whose associated $\mathbf{B}_{m,\boldsymbol{\theta}_S}$ has large trace value. For example, when there is only a single target in the scene, the $q \times q$ matrix $\mathbf{B}_{m,\boldsymbol{\theta}_S}$ degenerates to a scalar. The objective of minimizing $\text{tr}(\mathcal{I}^{-1}(\mathbf{p}, \boldsymbol{\theta}_S))$ is equivalent to maximizing $\mathcal{I}(\mathbf{p}, \boldsymbol{\theta}_S)$, which is $\sum_{m=1}^{M} p_m \mathbf{B}_{m,\boldsymbol{\theta}_S}$, and subject to the constraints of $\sum_{m=1}^{M} p_m = P$, $p_m \geq 0$ and $p_m \leq p_{max}$. This will lead to a result of assigning p_{max} to the transmitters with the first $\tilde{M}$ largest values of $\mathbf{B}_{m,\boldsymbol{\theta}_S}$, where $\tilde{M} = \lfloor P/p_{max} \rfloor$ and the remaining power $P - \tilde{M} p_{max}$ to the transmitter with the next largest $\mathbf{B}_{m,\boldsymbol{\theta}_S}$. When there are multiple targets in the field, the allocation is not as simple and must be determined by the optimization algorithms. Nonetheless one can still expect that the transmitters with large trace of $\mathbf{B}_{m,\boldsymbol{\theta}_S}$ be allocated more power than those with small trace of $\mathbf{B}_{m,\boldsymbol{\theta}_S}$.

IV. Grouped-coordinate Descent Reconstruction with Dynamic Dictionary

For a multistatic RF imaging system, image reconstruction is to estimate the unknown vector $\boldsymbol{\theta}$ from the set of noisy observations $\{\mathbf{y}_{mn}\}$. Like most other image reconstruction techniques, it is an inverse problem which can be solved by

Algorithm 2 Grouped-coordinate Descent Reconstruction with Dynamic Dictionary

Input: $\{\mathbf{y}_{mn}\}$, $\{\mathbf{D}_{mn}\}$, $\mathbf{p}$, N_{iter}, ϵ
Init: $\boldsymbol{\theta}^{(0)} = \arg\min_{\boldsymbol{\theta}} \sum_m \sum_n \left|\mathbf{y}_{mn} - \sqrt{p_m}\mathbf{D}_{mn}\boldsymbol{\theta}\right|^2 + \lambda|\boldsymbol{\theta}|_1$
    $S = \{k : \theta_k^{(0)} > \theta_{\text{min}}\}$ and $\tilde{S} = \{1, 2, \ldots, K\} - S$
    $\tilde{\mathbf{D}}_{mn}^{(0)} = \{\text{Echoes of the second order reflections via } \mathbf{x}_S\}$
while $i < N_{iter}$ and $|\boldsymbol{\theta}^{(i)} - \boldsymbol{\theta}^{(i-1)}| > \epsilon$ **do**
    $\boldsymbol{\theta}_S^{(i)} = \arg\min_{\boldsymbol{\theta}_S} \sum_m \sum_n \left|\mathbf{y}_{mn} - \sqrt{p_m}\left(\mathbf{D}_{mn,S}\boldsymbol{\theta}_S + \mathbf{D}_{mn,\tilde{S}}\boldsymbol{\theta}_{\tilde{S}}^{(i-1)} + \tilde{\mathbf{D}}_{mn}^{(i-1)}\mathbf{v}(\boldsymbol{\theta}_S^{(i-1)})\right)\right|^2 + \lambda|\boldsymbol{\theta}_S|_1$
    $\boldsymbol{\theta}_{\tilde{S}}^{(i)} = \arg\min_{\boldsymbol{\theta}_{\tilde{S}}} \sum_m \sum_n \left|\mathbf{y}_{mn} - \sqrt{p_m}\left(\mathbf{D}_{mn,S}\boldsymbol{\theta}_S^{(i)} + \mathbf{D}_{mn,\tilde{S}}\boldsymbol{\theta}_{\tilde{S}} + \tilde{\mathbf{D}}_{mn}^{(i-1)}\mathbf{v}(\boldsymbol{\theta}_S^{(i)})\right)\right|^2 + \lambda\left|\boldsymbol{\theta}_{\tilde{S}}\right|_1$
    $S = \{k : \theta_k^{(i)} > \theta_{\text{min}}\}$ and $\tilde{S} = \{1, 2, \ldots, K\} - S$
    $\tilde{\mathbf{D}}_{mn}^{(i)} = \{\text{Echoes of the second order reflections via } \mathbf{x}_S\}$
    $i = i + 1$
end while
Output: $\boldsymbol{\theta}^{(i)}$, S

statistical methods, such as maximum likelihood (ML), penalized maximum likelihood (PML), or maximum *a posteriori* methods. These methods usually generate reconstructions with less variance relative to filtered backprojection. The quality of reconstructions using purely the ML criterion is poor due to artifacts and noise. Regularization or a penalty is often added to the objective function to reduce the noise and artifacts, which is called penalized maximum likelihood. Assuming sparse targets in the field, it is natural to use l_1 norm of $\boldsymbol{\theta}$ as a regularizer to encourage sparsity of the solution [40].

Sparse representation and reconstruction have been widely studied to efficiently sample and reconstruct sparse signals [41]–[43]. An efficient dictionary is important in sparse representation and reconstruction. Various dictionary learning rules have been developed for different applications. The problem is generally formulated as

$$\min_{\mathbf{D},\boldsymbol{\theta}} \frac{1}{2}|\mathbf{y} - \mathbf{D}\boldsymbol{\theta}|^2 + \lambda|\boldsymbol{\theta}|_1 \tag{11}$$

where $\mathbf{y}$ is the observation, $\mathbf{D}$ is the dictionary to be learnt, $\boldsymbol{\theta}$ is the signal or parameter to be estimated, and $\lambda > 0$ is the coefficient which controls the weight of the regularizer. $|\cdot|_1$ represents l_1 norm of a vector. When $\mathbf{D}$ is known, the problem is commonly known as least absolute shrinkage and selection operator (LASSO) [44]. Sparse reconstruction with a dynamic dictionary was studied for joint model order and parameter estimation in [45], [46]. The method iteratively selects a subset of dictionary to achieve model reduction. The reconstruction of RF imaging can be formulated as the following with fixed first and second order dictionaries,

$$\hat{\boldsymbol{\theta}} = \arg\min_{\boldsymbol{\theta}} \frac{1}{2}\sum_{m=1}^{M}\sum_{n=1}^{N}\left|\mathbf{y}_{mn} - \sqrt{p_m}\left(\mathbf{D}_{mn}\boldsymbol{\theta} + \tilde{\mathbf{D}}_{mn}\mathbf{v}(\boldsymbol{\theta})\right)\right|^2 + \lambda|\boldsymbol{\theta}|_1 \tag{12}$$

As discussed previously, the number of elements of a full size second order dictionary $\tilde{\mathbf{D}}_{mn}$ is $\frac{K(K-1)}{2}$, it is impractical to use the dictionary due to the high computational cost caused by the large model size. This motivates the need to find an efficient model reduction method. As the secondary reflections from non-target pixels are much weaker than those from target pixels, $\tilde{\mathbf{D}}_{mn}$ can be built based on the secondary reflections from target pixels only. Due to the sparsity of targets, the size of a target driven secondary dictionary is much smaller than the full size dictionary.

It's well known that incorporation of prior knowledge about the distribution being imaged can accelerate statistical reconstruction [9], [47], [48]. As target location can be estimated from initial sensing, we propose a grouped-coordinate descent (GCD) type reconstruction algorithm to incorporate the target information. The algorithm iteratively updates the group of target location space parameters and the group of non-target location space parameters. In addition to the intrinsic fast convergence rate, the algorithm also allows iterative introduction and pruning of elements in the secondary dictionary according to the estimated target locations, which significantly reduces the size of the dictionary, and thus the computational complexity of reconstruction caused by modeling the second order reflections. The iterative optimization procedure with cyclic fixing of groups of parameters and optimizing over remaining parameters was first introduced by Jensen etc. for maximizing likelihood functions [49]. Fessler formally named the procedure as grouped-coordinate ascent (GCA) algorithm to distinguish it from his previous work of space alternating generalized expectation-maximization, which is a single-coordinate ascent (SCA) type algorithm for image reconstruction of emission tomography [50]–[52]. The global convergence and the asymptotic convergence rates of this method were established by Xu and Yin [53], [54]. They renamed the procedure as block coordinate descent, and applied it in nonconvex optimization [54]. Other than the fast convergence rate, GCD type algorithms are also easily parallelizable, which is a key attribute to enable real time applications.

The pseudocode of the reconstruction algorithm is given in Algorithm 2. The algorithm takes the set of RF measurements $\{\mathbf{y}_{mn}\}$ and the set of the first order dictionaries $\mathbf{D}_{mn}$ as input. After the first reconstruction, $\boldsymbol{\theta}^{(0)}$ has large values at target and ghost target locations. Target set S is estimated based on a threshold, $S := \{k|\theta_k^{(0)} > \theta_{\text{min}}\}$. Please note S is updated in each iteration although the iteration number is omitted to avoid confusion. Dictionary elements corresponding to the secondary

This article has been accepted for publication in a future issue of this journal, but has not been fully edited. Content may change prior to final publication. Citation information: DOI 10.1109/TAES.2021.3098160, IEEE Transactions on Aerospace and Electronic Systems

reflections from target locations $\mathbf{x}_S$ are added to $\tilde{\mathbf{D}}_{mn}^{(0)}$. The total number of elements in $\tilde{\mathbf{D}}_{mn}^{(0)}$ equals $q(q-1)/2$. During the i-th iteration, θ is split into two groups, i.e. the group of target space parameters $\theta_S^{(i)}$ and the group of non-target space parameters $\theta_{\tilde{S}}^{(i)}$. The two groups of parameters are updated sequentially to speed up the convergence. Target set S and the secondary order dictionary $\tilde{\mathbf{D}}_{mn}^{(i)}$ are updated according to the value of $\theta^{(i)}$. Once the stopping criteria is met, the algorithm outputs S as the target set and $\theta^{(i)}$ as the reconstructed image.

V. Numerical Simulations

To demonstrate the effectiveness of the proposed power allocation strategies and reconstruction algorithm, we have simulated the performance of the dynamic data driven multistatic RF imaging system in different scenarios. While the derivation in this paper doesn't assume a specific geometric setup of the multistatic RF imaging system, the numerical simulations are based on the sensor distributions of two distributed sensing research facilities. Fig. 2 shows aerial

(a) Tillman (b) Stockbridge

Fig. 2: Distributed sensing facilities in AFRL.

views of the two facilities. The facility shown in Fig. 2 (a) is named Tillman, while the facility in Fig. 2 (b) is named Stockbridge. Tillman is in a city environment, and composed of 12 radar sensors pseudo randomly distributed on a circle of 80m radius. Each sensor is mounted on a tower and elevated 15.24m above the ground. The sensor is capable to transmit arbitrary waveforms between 200MHz and 1GHz. Stockbridge occupies 300 acres of rural land. It's electromagnetically more quiet than Tillman, and composed of 24 radar sensors pseudo randomly located in the field [55]. Both facilities can perform a variety of experiments including the generation of complex EM environment, RF tomography, radar imaging, hybrid sensor imaging and distributed sensing.

To simulate the echoes received by the multistatic RF sensors, first order dictionaries for the bistatic links in Tillman and Stockbridge are pre-calculated and multiplied with the target and non-target reflectivity coefficients. The secondary reflections are simulated according to the target locations in each simulation. Zero mean stationary Gaussian noise is added to achieve desired signal to noise ratios.

A. Power allocation

Using the estimated target locations and sensor locations, optimal power allocations are calculated for the two scenarios discussed in Section III, i.e. mean squared error minimization and total power minimization, separately. Three power allocation strategies including uniform power allocation, greedy power allocation and optimal power allocation, are compared. The greedy strategy is calculated based on the heuristic approach aforementioned.

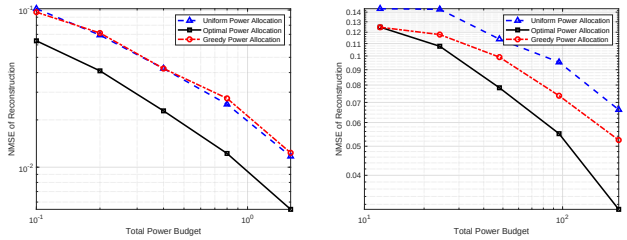

(a) Tillman (b) Stockbridge

Fig. 3: Comparison of power allocation strategies to minimize mean squared error of reconstruction.

Fig. 3 shows the performance of the three power allocation strategies in the scenario of minimizing mean squared error of reconstruction. A total of 500 Monte Carlo simulations of 5 randomly located targets have been generated at each level of power budget. Although different power allocation strategies lead to different energy of the received RF echoes, the total power budget and the noise level remain the same for all the 3 strategies to make fair comparisons. As it can be clearly seen from the Fig. 3, the Fisher information based optimal power allocation yields the best reconstruction accuracy as compared to the other two power allocation strategies in both Tillman and Stockbridge. The reconstruction accuracy of greedy power allocation is similar to that of uniform power allocation in Tillman, and is better than uniform power allocation in Stockbridge. We think the performance difference of greedy power allocation in the two setups is due to the change in sensor distribution topology. Sensors in Tillman are distributed on a ring in a smaller area than Stockbridge. A target in a random location in Tillman may have similar distances to several sensors, while a target in a random location in Stockbridge has a higher chance to be closer to a specific sensor than any other sensors. As greedy power allocation favors nearest transmitting sensor, the sensor distribution in Stockbridge may give advantages to greedy power allocation over uniform allocation. Further investigation is needed to validate this conjecture.

The comparison of the three power allocation strategies to minimize total power budget given a required reconstruction accuracy is shown in Fig. 4. The Fisher information based power allocation has again performed better than the other two strategies. In both Tillman and Stockbridge setups, the optimal power allocation needs less power budget than the other two strategies to achieve a specified reconstruction accuracy. As the sensors in Stockbridge are distributed in a much larger field, it's reasonable that more power is needed in Stockbridge than Tillman to achieve the same reconstruction accuracy. It's worth noting that greedy power allocation performs worse than uniform power allocation in both Tillman and Stockbridge in

This article has been accepted for publication in a future issue of this journal, but has not been fully edited. Content may change prior to final publication. Citation information: DOI 10.1109/TAES.2021.3098160, IEEE Transactions on Aerospace and Electronic Systems

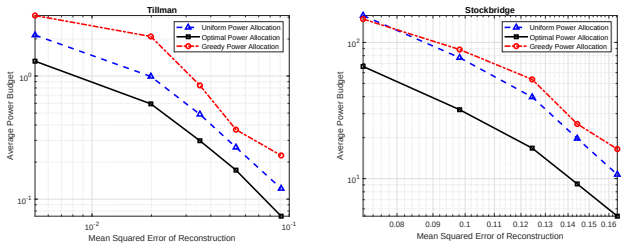

(a) Tillman (b) Stockbridge

Fig. 4: Comparison of power allocation strategies to minimize total power consumption.

this scenario, while the performance gap in Stockbridge is smaller than that in Tillman. The sensor distribution topology may play a similar role as discussed above.

B. Reconstructions

Two experiments have been performed to demonstrate the advantages of the proposed reconstruction algorithm. In the first experiment, a scene of 5 targets randomly located in Tillman is simulated without noise. Two reconstructions, one using only first order dictionary, while the other using both the first order dictionary and the dynamically built secondary dictionary, are performed. Fig. 5 shows the results of the two reconstructions. The reconstruction assisted by the secondary dictionary has much less artifacts than the reconstruction using only first order dictionary.

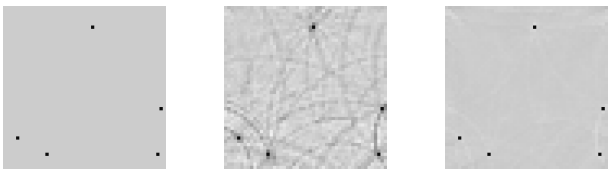

(a) Original image (b) First order dictionary only (c) First and second order dictionaries

Fig. 5: Comparison of reconstruction accuracy using different order dictionaries.

In the second experiment, the convergence rate of the grouped-coordinate descent (GCD) reconstruction algorithm is compared to that of the single coordinate descent (SCD) reconstruction algorithm. The scene is the same as the first experiment, but Gaussian noise is added to the simulated echoes. Both algorithms use dynamic secondary dictionary to improve reconstruction accuracy. Fig. 6 shows the residual error of the two algorithms after different number of iterations. It's clear that the GCD reconstruction algorithm converges faster than the SCD algorithm. The reconstruction results of the GCD algorithm after 4, 8, 12, 16 and 20 number of iterations are shown in Fig. 7. The reconstruction quality increases with the number of iterations, which confirms the convergence of the algorithm. Artifacts have been greatly reduced after 20 iterations.

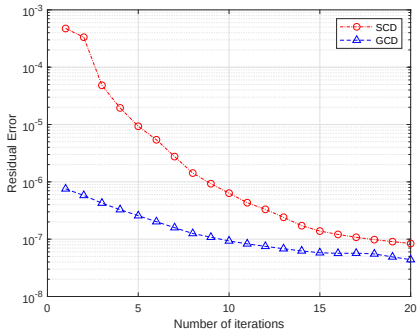

Fig. 6: Comparison of convergence rate of SCD and GCD algorithms.

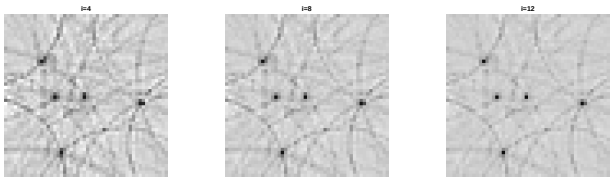

(a) $i = 4$ (b) $i = 8$ (c) $i = 12$

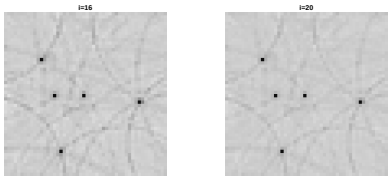

(d) $i = 16$ (e) $i = 20$

Fig. 7: Reconstruction results of GCD algorithm after different number of iterations.

C. Dynamic Data Driven RF Imaging

Finally, the entire dynamic data driven RF imaging system is simulated using the sensor setup at Tillman. Figure 8 illustrates the implementation of dynamic power allocation through a feedback loop in the RF imaging system. Assuming a fixed total power used by the imaging system, uniform power allocation is applied to obtain the echoes in initial sensing. The first image reconstruction is performed using only the fixed first order dictionary. After target locations are estimated from the first reconstruction, the power allocation is updated and new echoes are simulated based on the updated power allocation. Then Algorithm 2, grouped-coordinate descent with dynamic dictionary is used to reconstruct the reflectivity of

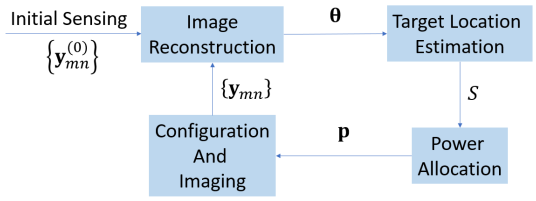

Fig. 8: RF imaging system with dynamic power allocation.

This article has been accepted for publication in a future issue of this journal, but has not been fully edited. Content may change prior to final publication. Citation information: DOI 10.1109/TAES.2021.3098160, IEEE Transactions on Aerospace and Electronic Systems

the scene. Fig. 9 shows a snapshot of the performance of the

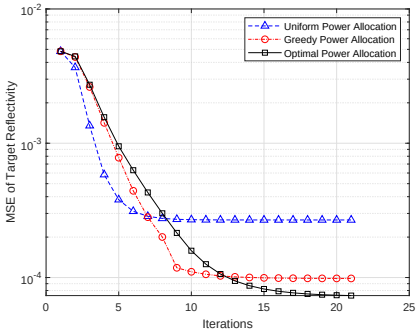

Fig. 9: Reconstruction accuracy of dynamic data driven RF imaging system with fixed total power budget.

dynamic data driven imaging system under different power allocation strategies. Three targets were randomly distributed in the scene. The mean squared error of reconstructed target reflectivity generally decreases with the number of reconstruction iterations. The accuracy of the first iteration is the same for all three power allocation strategies because reconstruction from initial sensing is the same regardless of the strategies. After that, the accuracy of uniform power allocation quickly converges in about 8 iterations, while the accuracy of greedy and optimal power allocations continuously to improve. The accuracy of optimal power allocation converges after 18 iterations and achieves the best result. Although the imaging accuracy varies with the target locations, the optimal power allocation strategy always achieve the best accuracy, while the greedy strategy and uniform strategy may beat each other depending on target locations.

We have also investigated whether the imaging system's performance changes with the number of targets in the scene. When using only the first order dictionary, imaging accuracy deteriorates with increasing number of targets, which is expected as the second order reflections were not modeled and become disturbance in the received echoes. When dynamic dictionary is used to include the second order reflections, imaging accuracy may vary with target locations, but does not show significant changes with the number of targets.

VI. Conclusions

The principle of dynamic data driven applications systems has been applied to improve the performance of multistatic RF imaging system. Target location information derived from initial sensing is exploited to optimally allocate power to transmitting sensors for target reflectivity estimation. Fisher information based optimization strategies are designed for two scenarios. One is to minimize the mean squared error of reconstruction given a fixed power budget, while the other is to minimize the total power consumption given a specified reconstruction accuracy. The numerical simulations show that the proposed power allocation strategies perform better than both uniform power allocation and greedy power allocation in the two scenarios. The proposed grouped-coordinate descent reconstruction algorithm incorporates target information to improve model fidelity and convergence rate. The dynamic second order dictionary helps to reduce the artifacts in reconstruction while maintains a practical model size and computational complexity. The algorithm converges faster than the traditional single coordinate descent algorithm and can be easily parallelized. In the future work, we will explore the impacts of sensor distribution topology to the power allocation strategy, and the reflectivity estimation of anisotropic scatterers in multistatic RF imaging.

Appendix
Derivation of Fisher information matrix

Consider the discrete first order model of the (m,n)-th bistatic pair. The observation $\mathbf{y}_{mn}$ has a multivariate normal distribution conditioned on known reflectance $\boldsymbol{\theta}$, which is shown in Eq. (5). The Fisher information matrix $\mathcal{I}_{mn}(p_m,\boldsymbol{\theta})$ is derived as follows.

$$
\begin{aligned}
&\mathcal{I}_{mn}(p_m,\boldsymbol{\theta})\\
=&\mathrm{E}\left[\left(\frac{\partial \log f(\mathbf{y}_{mn};\boldsymbol{\theta})}{\partial\boldsymbol{\theta}}\right)\left(\frac{\partial \log f(\mathbf{y}_{mn};\boldsymbol{\theta})}{\partial\boldsymbol{\theta}}\right)^T\middle|\boldsymbol{\theta}\right]\\
=&\frac{1}{4\sigma_\omega^4}\mathrm{E}\left[\left(\frac{\partial|\mathbf{y}_{mn}-\sqrt{p_m}\mathbf{D}_{mn}\boldsymbol{\theta}|^2}{\partial\boldsymbol{\theta}}\right)\cdot\right.\\
&\left.\left(\frac{\partial|\mathbf{y}_{mn}-\sqrt{p_m}\mathbf{D}_{mn}\boldsymbol{\theta}|^2}{\partial\boldsymbol{\theta}}\right)^T\middle|\boldsymbol{\theta}\right]\\
=&\frac{1}{\sigma_\omega^4}p_m\mathbf{D}_{mn}^T\cdot\\
&\mathrm{E}\left[(\mathbf{y}_{mn}-\sqrt{p_m}\mathbf{D}_{mn}\boldsymbol{\theta})(\mathbf{y}_{mn}-\sqrt{p_m}\mathbf{D}_{mn}\boldsymbol{\theta})^T\middle|\boldsymbol{\theta}\right]\mathbf{D}_{mn}\\
=&\frac{p_m\mathbf{D}_{mn}^T\mathbf{D}_{mn}}{\sigma_\omega^2}
\end{aligned}
\tag{13}
$$

Assuming the noise of each channel is independent, the Fisher information matrix over $\boldsymbol{\theta}$ by the whole multistatic imaging system is the sum over the Fisher information matrix of individual bistatic pairs due to the linearity of expectation and partial derivative,

$$
\begin{aligned}
\mathcal{I}(\mathbf{p},\boldsymbol{\theta})&=\sum_{m=1}^{M}\sum_{n=1}^{N}\mathcal{I}_{mn}(p_m,\boldsymbol{\theta})\\
&=\frac{1}{\sigma_\omega^2}\sum_{m=1}^{M}p_m\sum_{n=1}^{N}\mathbf{D}_{mn}^T\mathbf{D}_{mn}\\
&=\frac{1}{\sigma_\omega^2}\sum_{m=1}^{M}p_m\mathbf{B}_m
\end{aligned}
\tag{14}
$$

where $\mathbf{B}_m:=\sum_{n=1}^{N}\mathbf{D}_{mn}^T\mathbf{D}_{mn}$ is a $K\times K$ matrix.

Acknowledgment

This work was supported by an Air Force Research Lab Summer Faculty Fellowship in 2020. The views and conclusions contained herein are those of the authors and should not be interpreted as necessarily representing the official policies or endorsements, either expressed or implied, of the Air Force Research Laboratory or the U.S. Government.

REFERENCES

[1] M. C. Wicks, B. Himed, H. Bascom, and J. Clancy, "Tomography of moving targets (tmt) for security and surveillance," in *Advances in Sensing with Security Applications NATO Security Through Science Series*. Springer, 2006, vol. 2, pp. 323–339.

[2] L. Lo Monte, D. Erricolo, F. Soldovieri, and M. C. Wicks, "Radio frequency tomography for tunnel detection," *IEEE Trans. on Geoscience and Remote Sensing*, vol. 48, no. 3, pp. 1128–1137, 2010.

[3] B. Hamilton, X. Ma, R. Baxley, and S. Matechik, "Propagation modeling for radio frequency tomography in wireless networks," *IEEE Journal of Selected Topics in Signal Processing*, vol. 8, no. 1, pp. 55–65, 2014.

[4] M. Gottinger, M. Hoffmann, M. Christmann, M. Schutz, F. Kirsch, P. Gulden, and M. Vossiek, "Coherent automotive radar networks: The next generation of radar-based imaging and mapping," *IEEE Journal of Microwaves*, vol. 1, no. 1, pp. 149–163, Jan. 2021.

[5] H. D. Griffiths and C. J. Baker, "Fundamentals of tomography and radar," in *Advances in Sensing with Security Applications Series 2*. Springer, 2006, pp. 171–187.

[6] E. Blasch, S. Ravela, and A. Aved, Eds., *Handbook of Dynamic Data Driven Applications Systems*. Springer, 2018.

[7] D. Shen, J. Lu, P. Zulch, M. Disasio, G. Chen, Z. Wang, and R. Niu, "Joint manifold learning based distributed sensor fusion of image and radio-frequency data," in *2019 IEEE Aerospace Conference*, 2019, pp. 1–9.

[8] U. K. Majumder, E. P. Blasch, and D. A. Garren, *Deep Learning for Radar and Communications Automatic Target Recognition*. Artech House, 2020.

[9] J. R. Guerci, "Cognitive radar: A knowledge-aided fully adaptive approach," in *2010 IEEE Radar Conference*, 2010, pp. 1365–1370.

[10] J. S. Bergin, J. R. Guerci, R. M. Guerci, and M. Rangaswamy, "Mimo clutter discrete probing for cognitive radar," in *2015 IEEE Radar Conference*, 2015, pp. 1666–1670.

[11] S. Gogineni, M. Rangaswamy, B. D. Rigling, and A. Nehorai, "Cramér-rao bounds for UMTS-based passive multistatic radar," *IEEE Trans. on Signal Processing*, vol. 62, no. 1, pp. 95–106, 2014.

[12] A. O. Hero III, C. M. Kreucher, and D. Blatt, "Information theoretic approaches to sensor management," in *Foundations and Applications of Sensor Management*. Springer, 2008, pp. 33–57.

[13] A. O. Hero III and D. Cochran, "Sensor management: Past, present, and future," *IEEE Sensors Journal*, vol. 11, no. 12, pp. 3064–3075, Dec 2011.

[14] H. Godrich, A. P. Petropulu, and H. V. Poor, "Sensor selection in distributed multiple-radar architectures for localization: A knapsack problem formulation," *IEEE Trans. on Signal Processing*, vol. 60, no. 1, pp. 247–260, 2012.

[15] S. Joshi and S. Boyd, "Sensor selection via convex optimization," *IEEE Trans. on Signal Processing*, vol. 57, no. 2, pp. 451–462, 2009.

[16] H. Jamali-Rad, A. Simonetto, X. Ma, and G. Leus, "Distributed sparsity-aware sensor selection," *IEEE Trans. on Signal Processing*, vol. 63, no. 22, pp. 5951–5964, 2015.

[17] C. Shi, F. Wang, M. Sellathurai, J. Zhou, and S. Salous, "Low probability of intercept-based optimal power allocation scheme for an integrated multistatic radar and communication system," *IEEE Systems Journal*, vol. 14, no. 1, pp. 983–994, 2020.

[18] J. Yan, J. Dai, W. Pu, S. Zhou, H. Liu, and Z. Bao, "Quality of service constrained-resource allocation scheme for multiple target tracking in radar sensor network," *IEEE Systems Journal*, vol. 15, no. 1, pp. 771–779, March 2021.

[19] N. Viswanathan, S. Venkatesh, and D. Schurig, "Optimization of a sparse aperture configuration for millimeter-wave computational imaging," *IEEE Trans. on Antennas and Propagation*, vol. 69, no. 2, pp. 1107–1117, 2021.

[20] M. Leigsnering, F. Ahmad, M. G. Amin, and A. M. Zoubir, "Specular multipath exploitation for improved velocity estimation in through-the-wall radar imaging," in *Proc. of 2014 IEEE International Conference on Acoustic, Speech and Signal Processing (ICASSP)*, 2014, pp. 1060–1064.

[21] M. Leigsnering, F. Ahmad, M. Amin, and A. Zoubir, "Multipath exploitation in through-the-wall radar imaging using sparse reconstruction," *IEEE Trans. on Aerospace and Electronic Systems*, vol. 50, no. 2, pp. 920–939, April 2014.

[22] G. E. Smith and B. G. Mobasseri, "Analysis and exploitation of multipath ghosts in radar target image classification," *IEEE Trans. on Image Processing*, vol. 23, no. 4, pp. 1581–1592, April 2014.

[23] T. Cui, Y. Marzouk, and K. Willcox, "Data-driven model reduction for the bayesian solution of inverse problems," *International Journal for Numerical Methods in Engineering*, vol. 102, no. 5, pp. 966–990, 2014.

[24] B. Peherstorfer and K. Willcox, "Dynamic data-driven model reduction: adapting reduced models from incomplete data," *Advanced Modeling and Simulation in Engineering Sciences*, vol. 3, no. 11, 2016.

[25] L. Mainini and K. Willcox, "Surrogate modeling approach to support real-time structural assessment and decision making," *AIAA Journal*, vol. 53, no. 6, pp. 1612–1626, 2015.

[26] N. Patwari and P. Agrawal, "Effects of correlated shadowing: Connectivity, localization, and rf tomography," in *2008 International Conference on Information Processing in Sensor Networks (ipsn 2008)*, 2008, pp. 82–93.

[27] D. Lee and G. B. Giannakis, "A variational bayes approach to adaptive radio tomography," *IEEE Trans. on Signal Processing*, vol. 68, pp. 3779–3792, 2020.

[28] C. Kreucher, K. Kastella, and A. O. Hero, "Information-based sensor management for multitarget tracking," in *Signal and Data Processing of Small Targets 2003*, O. E. Drummond, Ed., vol. 5204, International Society for Optics and Photonics. SPIE, 2004, pp. 480–489.

[29] F. Zhao, J. Shin, and J. Reich, "Information-driven dynamic sensor collaboration," *IEEE Signal Processing Magazine*, vol. 19, no. 2, pp. 61–72, March 2002.

[30] J. L. Williams, J. W. Fisher III, and A. S. Willsky, "Performance guarantees for information theoretic active inference," in *Proceedings of the Eleventh International Conference on Artificial Intelligence and Statistics*, ser. Proceedings of Machine Learning Research, M. Meila and X. Shen, Eds., vol. 2. PMLR, 2007, pp. 620–627.

[31] W. W. Schmaedeke, "Information-based sensor management," in *Signal Processing, Sensor Fusion, and Target Recognition II*, I. Kadar and V. Libby, Eds., vol. 1955, International Society for Optics and Photonics. SPIE, 1993, pp. 156–164.

[32] M. L. Hernandez, T. Kirubarajan, and Y. Bar-Shalom, "Multisensor resource deployment using posterior cramer-rao bounds," *IEEE Trans. on Aerospace and Electronic Systems*, vol. 40, no. 2, pp. 399–416, April 2004.

[33] T. Kangsheng and Z. Guangxi, "Sensor management based on Fisher information gain," *Journal of Systems Engineering and Electronics*, vol. 17, no. 3, pp. 531–534, 2006.

[34] J. Denzler and C. M. Brown, "Information theoretic sensor data selection for active object recognition and state estimation," *IEEE Trans. on Pattern Analysis and Machine Intelligence*, vol. 24, no. 2, pp. 145–157, Feb 2002.

[35] C. Kreucher, K. Kastella, and A. O. Hero, "Multi-target sensor management using alpha-divergence measures," in *Information Processing in Sensor Networks*, F. Zhao and L. Guibas, Eds. Berlin, Heidelberg: Springer Berlin Heidelberg, 2003, pp. 209–222.

[36] C. Yang, L. Kaplan, E. Blasch, and M. Bakich, "Optimal placement of heterogeneous sensors for targets with gaussian priors," *IEEE Trans. on Aerospace and Electronic Systems*, vol. 49, no. 3, pp. 1637–1653, 2013.

[37] S. Boyd and L. Vandenberghe, *Convex Optimization*. Cambridge University Press, 2004.

[38] J. Bergstra and Y. Bengio, "Random search for hyper-parameter optimization," *Journal of Machine Learning Research*, vol. 13, pp. 281–305, 2012.

[39] M. Andersen, J. Dahl, and L. Vandenberghe. [Online]. Available: https://cvxopt.org

[40] B. Zhang, X. Cheng, N. Zhang, Y. Cui, Y. Li, and Q. Liang, "Sparse target counting and localization in sensor networks based on compressive sensing," in *2011 Proceedings IEEE INFOCOM*, 2011, pp. 2255–2263.

[41] R. Tibshirani, "Regression shrinkage and selection via the lasso," *Journal of the Royal Statistical Society*, vol. 58, no. 1, pp. 267–288, 1996.

[42] S. S. Chen, D. L. Donoho, and M. A. Saunders, "Atomic decomposition by basis pursuit," *SIAM J. Sci. Comput.*, vol. 20, no. 1, pp. 33–61, 1998.

[43] S. J. Wright, R. D. Nowak, and M. A. T. Figueiredo, "Sparse reconstruction by separable approximation," *IEEE Trans. on Signal Processing*, vol. 57, no. 7, pp. 2479–2493, July 2009.

[44] R. Tibshirani, "Regression shrinkage and selection via the lasso," *Journal of the Royal Statistical Society. Series B (Methodological)*, vol. 58, no. 1, pp. 267–288, 1996.

[45] C. D. Austin, J. N. Ash, and R. L. Moses, "Parameter estimation using sparse reconstruction with dynamic dictionaries," in *Proc. of 2011 IEEE International Conf. on Acoustics, Speech and Signal Processing*, 2011, pp. 2852 – 2855.

[46] C. D. Austin, J. N. Ash, and R. L. Moses, "Dynamic dictionary algorithms for model order and parameter estimation," *IEEE Trans. on Signal Processing*, vol. 61, no. 20, pp. 5117–5130, 2013.

[47] H. M. Hudson and R. S. Larkin, "Accelerated image reconstruction using ordered subsets of projection data," *IEEE Trans. on Medical Imaging*, vol. 13, no. 4, pp. 601–609, 1994.
[48] B. F. Hutton, H. M. Hudson, and F. J. Beekman, "A clinical perspective of accelerated statistical reconstruction," *European Journal of Nuclear Medicine volume*, vol. 24, pp. 797–808, 1997.
[49] S. T. Jensen, S. Johansen, and S. L. Lauritzen, "Globally convergent algorithms for maximizing likelihood function," *Biometrika*, vol. 78, no. 4, pp. 867–877, 1991.
[50] J. A. Fessler and A. O. Hero, "Space-alternating generalized expectation-maximization algorithm," *IEEE Trans. on Signal Processing*, vol. 42, no. 10, pp. 2664–2677, 1994.
[51] ——, "Penalized maximum-likelihood image reconstruction using space-alternating generalized EM algorithms," *IEEE Trans. on Image Processing*, vol. 4, no. 10, pp. 1417–1429, 1995.
[52] J. A. Fessler, E. P. Ficaro, N. H. Clinthorne, and K. Lange, "Grouped-coordinate ascent algorithms for penalized-likelihood transmission image reconstruction," *IEEE Trans. on Medical Imaging*, vol. 16, no. 2, pp. 166–175, 1997.
[53] Y. Xu and W. Yin, "A block coordinate descent method for regularized multiconvex optimization with applications to nonnegative tensor factorization and completion," *SIAM Journal on Imaging Sciences*, vol. 6, no. 3, pp. 1758–1789, 2013.
[54] ——, "A globally convergent algorithm for nonconvex optimization based on block coordinate update," *Journal of Scientific Computing*, vol. 72, no. 2, pp. 700–734, 2017.
[55] [Online]. Available: https://www.griffissinstitute.org/who-we-work-with/afrl/stockbridge-test-facility-brochure

Robert Ewing Dr. Ewing (S'77-M'87-SM'02-F'14) began his career in the Propulsion Laboratory at Wright-Patterson Air Force Base (Dayton, Ohio) with the development of high-speed jet engine control systems. He later held the position of a medical research scientist at the Aerospace Medical Research Laboratory and Instructor at the Air Force Institute of Technology (AFIT), where he co-pioneered the use of Quantitative Feedback Theory (QFT) for the design of robust analog and digital flight control and aircraft ejection systems. During the early 90's, Dr. Ewing led the Wright Laboratory's Solid State Electronic Devices Directorate's research in the area of mixed-signal hardware description language (VHDL-AMS) for microelectronic VLSI digital design, the IEEE VHDL standards and formal verification of digital designs. He became the Director of the Computer Engineering Research Consortium, a research center composed of universities, industry and graduate students for the innovative development of mixed-signal design methodology and tools, real-time wavelet transforms for video and radar applications, and Spiking Neural Networks for Pattern Recognition. He has authored over 140 journal and conference publications, chaired numerous international IEEE conferences, Adjunct Professor, Associate Editor for Electronic Letters, The Institute of Engineering and Technology (IET) Journal, and Board of Governors, Executive Director, IEEE Aerospace and Electronics Systems Society.

Erik Blasch Erik Blasch is an Air Force Research Laboratory Program Officer. He received his B.S. in Mechanical Engineering from the Massachusetts Institute of Technology and PhD. In Electrical Engineering from Wright State University with Master's degrees in ME, Industrial Eng., Health Science, EE, Medicine, Military Studies, Economics, and Business. Additionally, his assignments include Colonel (ret) in the USAF reserves and adjunct associate professor with interests in information fusion and human-machine integration, compiling 900+papers, 35 patents, and 8 books. He is an Associate Fellow of AIAA, Fellow of SPIE, and Fellow of IEEE.

Jia Li Jia Li received her B.S. degree in electronics and information systems from Peking University, Beijing, China, in 1996, the M.S.E. degree, and the Ph.D. degree both in electrical engineering from the University of Michigan, Ann Arbor, MI, in 1997 and 2002, respectively. She has been a faculty member in the School of Engineering and Computer Science at Oakland University since 2002. Her research interests are in the areas of statistical learning and signal processing with applications in radar, sensor fusion, communications and biomedical imaging. She has authored/co-authored over 70 referred publications, including one book. Her past and current research are sponsored by NSF, NIH, General Motors, Fiat Chrysler, National Research Council, and Air Force Office of Scientific Research. Dr. Li serves as a member of technical committees of several international conferences and workshops. She is a senior member of IEEE.